



Positive effects of phosphotungstic acid on the in-situ solid-state polymerization and visible light photocatalytic activity of polyimide-based photocatalyst



Pengcheng Meng, Huimin Heng, Yanhong Sun, Junhao Huang, Jinpeng Yang, Xia Liu*

College of science, China Agricultural University, Beijing, 100193, PR China

ARTICLE INFO

Keywords:
Visible-light-driven
Polymerization
Phosphotungstic acid
Polyimide
Imidacloprid

ABSTRACT

A series of $H_3PW_{12}O_{40}$ (HPW)-containing polyimide (PI) hybrid composites (TPI) are prepared through in-situ solid-state polymerization using HPW, melem and pyromellitic dianhydride as precursors. The effect of HPW on the morphology, porosity, chemical structure, and optical and visible-light photocatalytic degradation efficiency of TPI composites are systematically investigated by various characteristic methods. By comparing the structure, property and photocatalytic activity of the TPI composites and the HPW-PI composites (prepared by the impregnation method), it indicates that HPW can promote the formation of C–N bond in the five-membered imide rings between amines and anhydrides during the in-situ solid-state condensation process. Subsequently, the visible-light ($\lambda > 400$ nm) photocatalytic degradation efficiency of imidacloprid on TPI composites is also enhanced compared with the pristine PI because of the enhancement of the in-situ solid-state condensation reaction, photogenerated electron-hole separation efficiency and visible-light utilization efficiency after the introduction of HPW. The visible-light photocatalytic degradation rate constant k of 15% TPI composites prepared at 300 °C and 5% TPI composites prepared at 325 °C are about 10.33 and 2.42 times of the corresponding pristine PI, respectively. Compared with commercial P25, the photocatalytic degradation efficiency of 15% TPI-300 and 5% TPI-325 are about 4.58 and 5.13 times of P25 under visible light irradiation.

1. Introduction

The photocatalytic degradation of organic pollutants in water, such as pesticide, dye, surfactant and pharmaceuticals [1–3], is the focus of environmental science. In the development of heterogeneous photocatalysts for water pollution remediation, the traditional inorganic semiconductor photocatalysts, like TiO_2 and ZnO [4–6], have been extensively investigated. However, their practical application will be limited by the weak visible light photocatalytic activity for their wide bandgap and weak visible light responsiveness. In recent years, the conjugated polymer-based photocatalysts has won widespread attention for their excellent photocatalytic activity, low cost and abundant sources [7]. The graphitic carbon nitride ($g-C_3N_4$) as an outstanding representative of conjugated polymer-based photocatalyst has been widely used in photocatalytic water splitting, degradation of organic pollutants and reduction of CO_2 for its suitable band structure and excellent visible light response [8–10]. Originally, polyimide (PI), as a special conjugated polymer engineering material, is widely used in the field of microelectronics, separation membranes and nanomaterials [11,12]. Reportedly, a polyimide prepared using melamine (MA) and

pyromellitic dianhydride (PMDA) can show excellent visible light response for its suitable band structure [13]. Even so, the photocatalytic degradation efficiency of PI is still low for the inherent transfer property and the persistent recombination of photogenerated carriers of polymer and its negative valence band (VB) potential compared to TiO_2 , ZnO , WO_3 and so on [14].

To improve the photocatalytic efficiency of PI, a series of strategies, including co-catalysts [14–17], heteroatoms doping [18,19], heterojunctions [19–25], are used to promote the separation of photogenerated electrons (e^-) and holes (h^+) or the positive shift of the valence band position. In detail, (i) for the co-catalysts represented by Pt and MoS_2 [14–17], they can be considered as electronic pools to suppress photogenerated carriers recombination [26]. (ii) The introduction of element S into the structural unit of PI, the conduction band (CB) and VB potential of PI will be significantly positive shifted [18,19]. (iii) The construction of heterojunctions in the form of hybrid composites is a worthwhile way to improve the photocatalytic oxidation capacity of photocatalysts [27]. As far as we know, catalysts that have been used to form heterojunctions with PI include tungsten oxide [19,20], $Zn_{0.25}Cd_{0.75}S$ [21], MoO_3 [22,23], ZnO [24] and $g-C_3N_4$ [25].

* Corresponding author at: College of science, China Agricultural University, Yuanmingyuan West Road No.2, Haidian District, Beijing, 100193, PR China.
E-mail addresses: pengchengmeng@126.com (P. Meng), liuxiacau@163.com (X. Liu).

This construction of such heterojunctions can suppress the photo-generated carriers recombination, and also enhance the visible-light utilization efficiency or the photocatalytic oxidation ability of PI on account of that their band structure are suitable for that of PI. However, phosphotungstic acid ($H_3PW_{12}O_{40}$, HPW) is an excellent homogeneous photocatalyst, also is an electronic acceptor or mediator for its excellent capability to accept or donate electrons with a well-defined Keggin structure [28,29]. Hence, the introduction of HPW into PI may suppress the photogenerated carriers recombination. Besides, due to the strong acidity and oxidation of phosphotungstic acid, it can catalyze many organic synthesis reactions, including esterification, oxidation and C–N bond formation [30–32]. The PI photocatalyst involved in this research is synthesized by imidization of amines and anhydrides [14]. Therefore, when HPW-containing PI hybrid composites (TPI) are prepared by in-situ solid-state polymerization using HPW with amines and anhydrides, HPW may promote the imidization of amines and anhydrides [32]. Given those assumption, it would be significant to investigate the incorporation of HPW and PI, and the effect of HPW on the synthesis and photocatalytic degradation efficiency of TPI composites.

Herein, a series of TPI composites are prepared through in-situ solid-state polymerization using HPW, MA and PMDA as precursors in this work. Due to the PI with different polymerization temperature will have different polymerization degree [16], so we study the effect of HPW on the in-situ solid-state polymerization by comparing the characterization results of TPI, HPW-PI and pristine PI with different polymerization temperature. Besides, the effect of HPW content on the morphology, adsorption capacity, chemical structure and optical properties of TPI composites are investigated by systematic characterization. The effect of HPW on the visible-light photocatalytic degradation efficiency of TPI composites are also systematically investigated. The possible photocatalytic mechanism are also proposed. The prepared TPI composites are expected to exhibit higher visible-light photocatalytic activity than pristine PI, because HPW can promote the formation of C–N bond between amines and anhydrides and can accept electrons.

2. Experimental

2.1. Chemicals and reagents

Melamine, pyromellitic dianhydride, phosphotungstic acid hydrate and ethyl acetate were purchased from Sinopharm Chemical Reagent Co., Ltd., China. Imidacloprid (98%) was provided by The Institute of Plant Protection, Chinese Academy of Agricultural Sciences. Deionized water was used in photocatalytic degradation of imidacloprid. All chemicals were analytical reagents and used without further purification.

2.2. Synthesis of melem

10 g of MA was put into a 40 mL porcelain crucible with a cover. Then, the crucible was calcined to 425 °C from room temperature in a muffle furnace with a heating rate of $10\text{ }^{\circ}\text{C min}^{-1}$ under ambient pressure in air. Keeping the temperature at 425 °C for 4 h, the melem was obtained after grinding, washing with deionized water and absolute ethyl alcohol and drying at 80 °C for 10 h in an air-circulating oven.

2.3. Synthesis of TPI composites

The TPI composites were prepared through an in-situ solid-state polymerization process in air. In a typical process, 2.182 g melem were dispersed in 20 mL ethyl acetate containing 0.230 g HPW under magnetic stirring to form a slurry. After stirring for 30 min, the slurry was treatment for 1 h in an ultrasonic bath and maintained the temperature at about 23 °C. Furthermore, 2.181 g PMDA were added into the slurry after continuing stirring 30 min. Then, the solvent was evaporated, and

the residues was dried at 80 °C for 10 h to obtain the TPI precursor. Moreover, the precursor of TPI was heated at 325 °C for 4 h with a rate of $10\text{ }^{\circ}\text{C min}^{-1}$. Finally, the resulting pale yellow solid powder was denoted as 5% TPI-325. According to this method, a series of x% TPI-y composites (x and y represent the HPW content in the precursor mixture and polymerization temperature, respectively) were prepared with different HPW content and polymerization conditions. Besides, the HPW content determined by ICP-MS in 15% TPI-300 and 5% TPI-325 composites are 14.22% and 4.87%, respectively. However, the pristine PI was also synthesized by the same method without adding HPW.

2.4. Synthesis of HPW-PI composites

The synthesis of HPW-PI composites was carried out by the impregnation method [33]. Typically, 0.105 g HPW was dissolved in deionized water, and then 2.000 g PI-325 was added into the HPW aqueous solution with stirring at ambient temperature for 12 h. Afterward, the water was evaporated at 80 °C, and the residues was dried continuously in the oven at 80 °C for 10 h to obtain the 5% HPW-PI-325 composites. Also, the 15% HPW-PI-300 composites was obtained using the same method.

2.5. Characterization

The crystalline structure of the pristine PI and TPI composites were confirmed by X-ray diffractometer (XRD, Bruker D8 ADVANCE diffractometer, Bruker AXS Company, Germany) using $Cu-K_{\alpha}$ radiation. The molecular structural information of the samples were analyzed by Fourier transform infrared spectroscopy (FT-IR, PerkinElmer Spectrum 100 FT-IR Spectrometer, PerkinElmer Optoelectronics, America) using KBr pellet support with the wavenumber range of $400\text{--}4000\text{ cm}^{-1}$. The morphologies and microstructures of TPI composites were examined with scanning electron microscope (SEM, Hitachi S-4800 electron microscope, Hitachi, Ltd., Japan) and transmission electron microscope (TEM, Tecnai G2 F20 electron microscope, FEI company, America) with a carbon-coated copper grid as the sample holder. The BET (Brunauer, Emmett and Teller) specific surface area was determined by N_2 adsorption–desorption isothermals (ASAP 2020, Micromeritics Instrument Corp, America). Meanwhile, the surface composition elements of the samples were detected with energy-dispersive X-ray spectra (EDS, HORIBA EX-350 spectrometer, Horiba, Ltd., Japan) equipped on the SEM. Furthermore, the accurate content of W in the TPI composites were analyzed by the inductively coupled plasma mass spectrometry (ICP-MS, Agilent 7500ce system, Agilent Technologies Inc., America). Also, the chemical state and valance band of the samples were obtained by X-ray photoelectron spectra (XPS, Thermo Scientific Escalab 250Xi X-ray photoelectron spectrometer, Thermo Fisher Scientific, America). The spectrum response range of the samples were measured by UV-vis diffuse reflectance spectra (UV-vis DRS, Specord 200 spectrophotometer, Analytikjena, Germany) using $BaSO_4$ as the reference. Moreover, The PL spectra were recorded on a FluoroMax-4 Spectrofluorometer (Horiba Jobin Yvon Inc., America) with an excitation wavelength of 325 nm.

2.6. Photocatalytic activity test

The photocatalytic activity of the pristine PI and TPI composites were evaluated by the degradation of imidacloprid under visible light ($\lambda > 400\text{ nm}$) irradiation [28,34]. Imidacloprid is a pervasive commercial neonicotinoid insecticide, and it has a negative impact on non-target species including humans [35]. Now, imidacloprid can be detected in surface and ground water for its water solubility (510 mg L^{-1} , 20 °C) and mobility [2]. The light source was a PLS-SXE300UV Xe lamp (15 A, 225 W). 1 mL samples was taken out from 50 mL imidacloprid aqueous solution at the specified time, and the imidacloprid concentration was detected after removal of the photocatalyst with a

0.22 μm filter. The degradation efficiency of imidacloprid was calculated according to the change of the concentration of imidacloprid in different samples. Also, the photocatalytic degradation of imidacloprid over pristine PI and TPI composites follows the pseudo-first-order kinetics model expressed by Langmuir-Hinshelwood model of $\ln(c_0/c) = kt$ [28,34], where c is the residual concentration at reaction time t , c_0 is the initial concentration, k is the pseudo-first order rate constant. Besides, the concentration of imidacloprid were detected with the liquid chromatography (LC) on an Agilent 1200 liquid chromatograph (Agilent Technologies Inc., America) equipped with an Agilent Eclipse XDB-C18 column ($4.6 \times 150 \text{ mm}$, particle size $5 \mu\text{m}$). Meanwhile, the mobile phase was a mixture of acetonitrile/water ($70:30, \text{v/v}$) at a flow rate of 1 mL min^{-1} , the injection volume was $20 \mu\text{L}$, and the detection wavelength was 270 nm .

2.7. Recyclability of TPI composites

In this section, 5% TPI-325 composites was chosen as a representative photocatalyst to evaluate the recyclability of TPI composites by the degradation of imidacloprid under visible light ($\lambda > 400 \text{ nm}$) irradiation. Typically, a similar photocatalytic degradation process was applied with the photocatalytic activity tests, except that the photocatalyst concentration was set at 2.5 g L^{-1} and the substrate concentration was 20 mg L^{-1} . The used photocatalysts were collected by centrifugation for recyclability tests. After the photocatalytic degradation reaction is completed, the photocatalysts were washed with distilled water and dried at 80°C for 10 h.

3. Results and discussion

3.1. The photocatalytic activity test

In order to obtain the HPW-containing polyimide photocatalyst with better photocatalytic degradation efficiency, a series of composites were prepared under different conditions, including the preparation method, HPW content, thermal polymerization temperature and time. By studying the influence of the above factors, from Fig. S1, it was found that 15% TPI-300 and 5% TPI-325 exhibited the best photocatalytic activity at their respective polymerization temperatures. From Fig. 1(a) and (b), the visible-light photocatalytic activity of the photocatalysts prepared by the in-situ polymerization method (15% TPI-300 and 5% TPI-325) are much higher than that of the photocatalysts prepared by the impregnation method (15% HPW-PI-300 and 5% HPW-PI-325). Also, the photocatalytic degradation efficiency of imidacloprid on the photocatalysts prepared by the impregnation method is higher than that of the respective pristine PI. Therefore, from Fig. 1, by comparing the photocatalytic activity of the photocatalysts prepared by the impregnation method and the in-situ polymerization method, it indicates that HPW may have some other roles in promoting the photocatalytic degradation capacity of the photocatalyst while promoting the separation of photogenerated carriers. In addition, from Fig. 1(c), the k of 15% HPW-PI-300 and 5% HPW-PI-325 is about 2.38 and 1.27 times that of the pristine PI-300 and PI-325, respectively. This may be due to the introduction of HPW to promote the separation of photogenerated carriers [36,37]. Fig. 1(c) demonstrates that the photocatalytic efficiency of imidacloprid on 15% TPI-300 and 5% TPI-325 are both more efficient than the pristine PI-325 (the highest photocatalytic efficiency photocatalyst in the pristine PIs) [14,16]. The k of 15% TPI-300 and 5% TPI-325 are about 10.50 and 19.33 times of PI-300, and are about 1.31 and 2.42 times of PI-325. On the other hand, the k of 15% TPI-300 and 5% TPI-325 is about 3.32 and 1.90 times that of the 15% HPW-PI-300 and 5% HPW-PI-325, respectively. Totally, based on the substantial enhanced photocatalytic activity of TPI composites, it indicates that HPW should have other effects in addition to being able to promote the separation of photogenerated carriers.

As we all know, the factors that affect the photocatalytic efficiency

are multifaceted. In detail, the composition, structural, morphological and optical changes of photocatalysts will all affect the photocatalytic degradation efficiency. Therefore, we chose the samples with the optimum photocatalytic efficiency at 300°C and 325°C respectively to investigate the reason for the difference of photocatalytic efficiency, and the specific reasons will be expounded in detail in the next few sections.

3.2. Structure of the samples

In order to investigate the effect of HPW on the structure and morphology of the samples, the FT-IR, XRD, XPS, N_2 adsorption-desorption, SEM and TEM were carried out.

The FT-IR spectra and XRD patterns of the samples were presented in Fig. 2. Totally, after in-situ thermal polymerization, the HPW in the TPI composites remained the original Keggin structure (Fig. 2Figs. 2 and S2), because the selected polymerization temperature is not sufficient to destroy the Keggin structure of HPW [38,39]. The polymerization degree changes can be indirectly showed from the changes of the peaks located at $1857, 1379$ and 902 cm^{-1} , and these three peaks are assigned to the characteristic absorption peaks of the anhydride precursor, the stretching vibration of $\text{C}-\text{N}-\text{C}$ in the five-membered imide rings and the stretching vibration of $\text{C}-\text{O}-\text{C}$ in the cyclic anhydride, respectively [13,14]. Specifically, as the polymerization degree increases, the peak at 1857 and 902 cm^{-1} gradually absent and the peak at 1379 cm^{-1} gradually attend. The peaks at $1771, 1715$ and 712 cm^{-1} are attributable to asymmetric stretching, symmetric stretching and bending vibration absorption peak of $\text{C}=\text{O}$ [13,15]. For PI-300, because the characteristic peaks of the anhydride precursors (the peak at 1857 and 902 cm^{-1}) are still faint presence, so PI-300 has an incomplete polymerization compared to PI-325 [13]. However, from Fig. 2(a) and (b), we found that the introduction of HPW could promote the polymerization between amine and anhydride precursors comparing with pristine PI. From Fig. 2(b), after the introduction of HPW, the more obvious presence of the peak at 1379 cm^{-1} (the stretching vibration peak of $\text{C}-\text{N}-\text{C}$ in the five-membered imide rings) provided a preliminary proof. As a comparison, the FT-IR spectra of 15% HPW-PI-300 and 5% HPW-PI-325 prepared by impregnation method were presented in Fig. 2(a), and the intensity of the peak at 1379 cm^{-1} of 15% HPW-PI-300 is as weak as PI-300. From the results of FT-IR spectra, HPW dose have a positive effect on the in-situ polymerization process of TPI composites.

For further verification, the XRD patterns of pristine PI, TPI composites and HPW-PI composites were analyzed. According to the reference, the higher diffraction peak intensity indicates that the stronger chain-to-chain interaction, more ordered chain orientation and the higher polymerization degree of the polyimide prepared by solid-state polymerization process [16]. Therefore, the XRD patterns of the samples can laterally reflect the polymerization process between amine and anhydride precursors. From Fig. 2(c), for pristine PI-325, there are several obvious characteristic diffraction peaks of pristine PI located at $26.9^\circ, 28.6^\circ$ and the range of $15^\circ\text{--}20^\circ$ [14,21]. Among, the characteristic peak intensity of PI at 28.6° reflecting the stacking of π -conjugated two-dimensional (2D) frameworks of PI [21]. For PI-300, the peak intensity of the peak at 28.6° is lower than that of PI-325. After the introduction of HPW, the characteristic peak of HPW appeared at about 6° , which can be obtained by comparing with the patterns of HPW-PI composites and the standard card of $\text{H}_3\text{PW}_{12}\text{O}_{40} \cdot 21\text{H}_2\text{O}$ (PDF #50-0655). Also, for 15% TPI-300, a significant presence of 28.6° peak indicates that HPW contributes to the polymerization of polyimide. Furthermore, the increase in the corresponding peak (peak at 28.6°) intensity of 5% TPI-325 can also verify this conclusion. By analyzing the results of FT-IR and XRD, it can be preliminarily determined that the introduction of HPW can significantly affect the synthesis of the samples. Especially, HPW can promote the polymerization between amine and anhydride precursors. The subsequent XPS spectra will be used to further

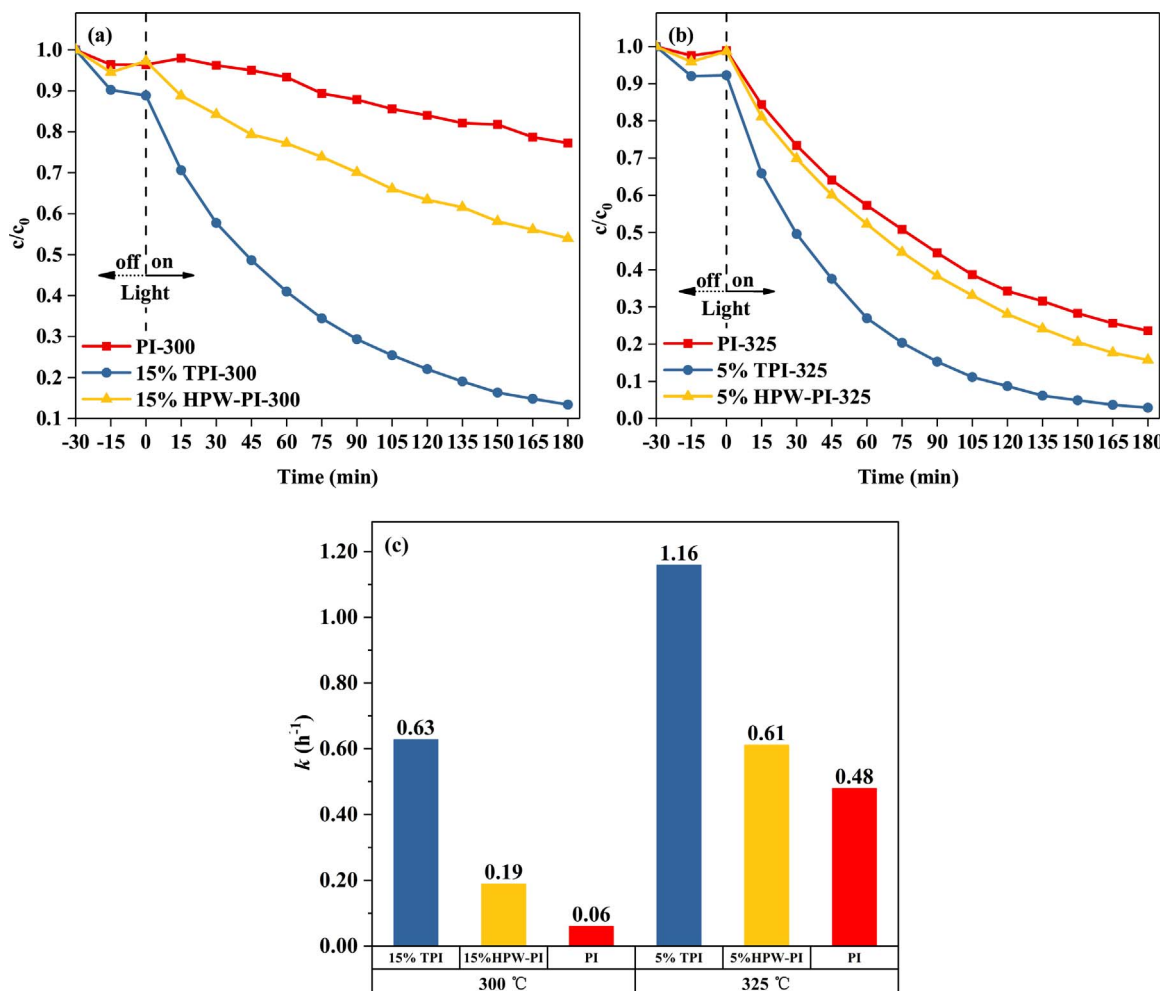


Fig. 1. The photocatalytic efficiency (a, b) and k (c) of TPI, HPW-PI and corresponding pristine PI. The imidacloprid concentration was 20 mg L⁻¹, the photocatalyst concentration was 1 g L⁻¹, $\lambda > 400$ nm.

investigate the effect of the introduction of HPW on structure of the samples.

Furthermore, the chemical state and elemental composition of the samples were analyzed by XPS spectra (Fig. 3). From the results of Fig. 3(a), there are only three elements in the pristine PI. After introducing HPW, the weak signal of W is detected for the low HPW content in TPI composites. Moreover, from Fig. 3(b), the W 4f peaks of 15% TPI-300 and 5% TPI-325 composites (W 4f_{7/2} 35.3 eV and W 4f_{5/2} 37.5 eV) have a negative shift compared to that of HPW (W 4f_{7/2} 36.1 eV and W 4f_{5/2} 38.3 eV). This means the electron density of HPW in TPI composites is increased after HPW captures electrons, and indicates that there is electron transfer between PI and HPW. Fig. 3(c) is the XPS N 1s spectra of pristine PI-300, PI-325, 15% TPI-300 and 5% TPI-325 composites. For PI-300, the N 1s peaks centered at 398.4, 399.7, 400.8 and 401.6 eV are attributed to the C=N-C in the tri-triazine ring, the C-N in the five-membered imide ring, the N-(C)₃ in the tri-triazine ring and unreacted amino (N-H), respectively [23,40,41]. From Fig. 3(c), only PI-300 is detected the signal of N-H for its low polymerization degree. And the proportion of C-N in the five-membered imide ring is significantly lower than that of PI-325, 15% TPI-300 and 5% TPI-325. Comparing the data of N 1s of PI-300 and 15% TPI-300, the increased proportion of C-N peak (at 399 eV) and the disappearance of N-H peak (at 401 eV) in the data of 15% TPI-300 can show that the introduction of HPW does promote the polymerization between amine and anhydride precursors. Moreover, the increase proportion of C-N in the five-membered imide ring can also be found in the comparison from the N 1s data of PI-325 and 5% TPI-325.

Correspondingly, the O1s data can also directly show that HPW has the effect of promoting polymerization between amine and anhydride precursors. From Fig. 3(d), the O 1s peaks centered at 531.5 and 533.0 eV are assigned to the C=O in the five-membered imide ring and C—O—C in the cyclic anhydride, respectively [42,43]. Also, the O 1s peaks centered at 530.2 and 532.2 eV are assigned to W—O—W and W—O—P in the Keggin structure of HPW, respectively [36,44]. Firstly, the presence of the peaks at 530.2 and 532.2 eV in the 15% TPI-300 and 5% TPI-325 O 1s spectra indicate that the successful introduction of HPW. Secondly, the changes in the C—O—C proportion can reflect the changes in the polymerization between amine and anhydride precursors. Comparing the O1s spectra among the 15% TPI-300, 5% TPI-325 and respective corresponding pristine PI, after introducing HPW, the peaks of C—O—C cannot be analyzed from the TPI composites O 1s spectra, and this indicates that the anhydride precursors are more polymerized with the amine precursors.

In summary, combined with the results of FT-IR, XRD and XPS, we can determined that the introduction of HPW can significantly affect the solid-state condensation between amine and anhydride precursors during the in-situ polymerization process of TPI composites. Based on the above results and related references, we try to propose how HPW positively affects the solid-state polymerization process between amine and anhydride. The fabrication of TPI composites and the photocatalytic mechanism in the TPI composites under visible-light irradiation are presented in Scheme 1. Firstly, HPW will be evenly dispersed in the precursor of TPI composites after the design treatment. Secondly, for the polymerization process of polyimide, the polyamic acid

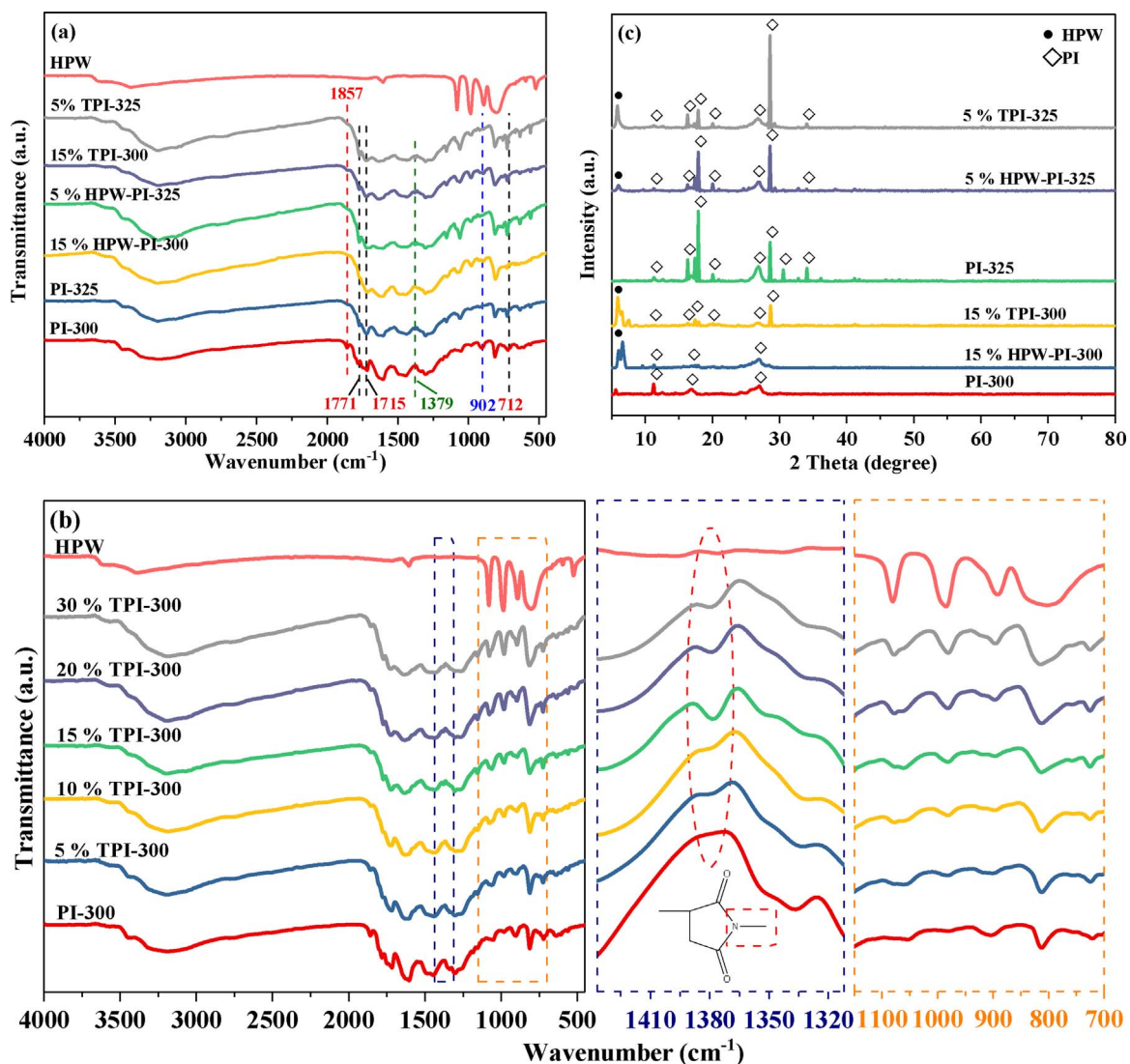


Fig. 2. FT-IR spectra of (a) HPW, 15% TPI-300, 5% TPI-325, corresponding HPW-PI composites and pristine PI, and (b) the TPI-300 composites with different HPW concentration. (c) XRD patterns of 15% TPI-300, 5% TPI-325, corresponding HPW-PI composites and pristine PI.

formation and the ring imidization are carried out simultaneously during the solid-state polymerization. The anhydride molecular is a molten state at the selected polymerization temperature and it will be react with the adjacent amine group of melem to form polyimide [23]. As shown in Scheme 1, it is reported that HPW can form the coordination activation with amine and anhydride during the preparation and thermal polymerization of the TPI precursor, and this coordination activation can facilitate the intermolecular ring imidization [45]. Simultaneously, the strong acidity of HPW can also promote the cyclo-dehydration process during the thermal imidization [32]. Hence, the efficiency of the polymerization will increase because of the introduction of HPW. Moreover, this effect will inevitably change the catalytic performance and morphology of the samples. Therefore, the SEM, TEM and the adsorption capacity tests of the samples were performed to investigate the changes on the morphology of the samples.

3.3. Morphology of the samples

From Fig. 4, it can be seen that both 15%TPI-300 (Fig. 4(a)) and 5%TPI-325 composites (Fig. 4(b)) exhibit lamellar stacking structures. For the different TPI composites, 15% TPI-300 exhibits a loose stack of laminations as compared to the tight stacking of 5% TPI-325. In addition, from the TEM images of the samples, 5% TPI-325 has a more

extensible lamellar structure than 15% TPI-300, which is due to the increased polymerization degree could facilitate the extension of the lamellar structure of the composites [13,16]. Besides, from the EDX elemental mappings of C, N, O and W, the HPW evenly distributed in the 15% TPI-300 and 5% TPI-325 composites, and this is conducive to the transfer of photogenerated carriers between PI and HPW [46,47].

Fig. 5(a) and (b) demonstrate the N₂ adsorption–desorption isotherms and the BET surface areas of the pristine PI, 5% TPI and 15% TPI composites prepared under 300 °C and 325 °C, respectively. All of the samples exhibit type IV isotherms with H3 hysteresis loop, and this indicates the mesoporous structure of pristine PI and TPI composites [36,37,48]. For the samples prepared under 300 °C (Fig. 5(a)), the BET surface areas gradually decrease as the HPW content increases from 5% to 15%. This decrease may be due to the increased polymerization degree caused by the introduction of HPW and the partially blocked pores [36]. However, for the samples prepared under 325 °C (Fig. 5(b)), the introduction of HPW has little effect on the BET surface areas of the samples. This is because the higher polymerization degree samples have already had a tight structure, which can be seen from the SEM and TEM images. This will make the effect of HPW on the BET surface areas of the samples is not obvious. Nevertheless, from the results of the adsorption capacity of pristine PI and TPI composites to imidacloprid (Fig. 5(c) and (d)), the removal efficiency of imidacloprid on TPI

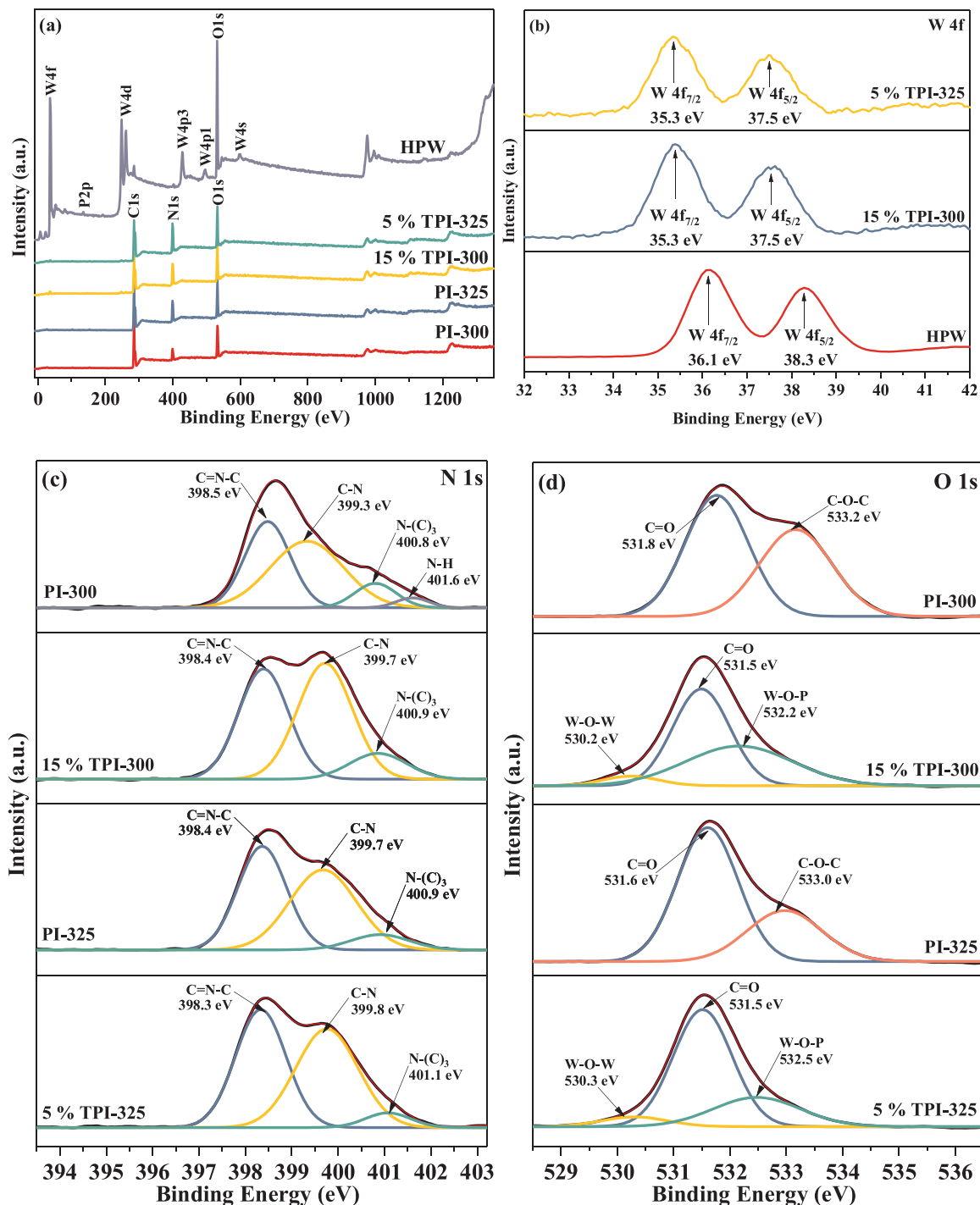


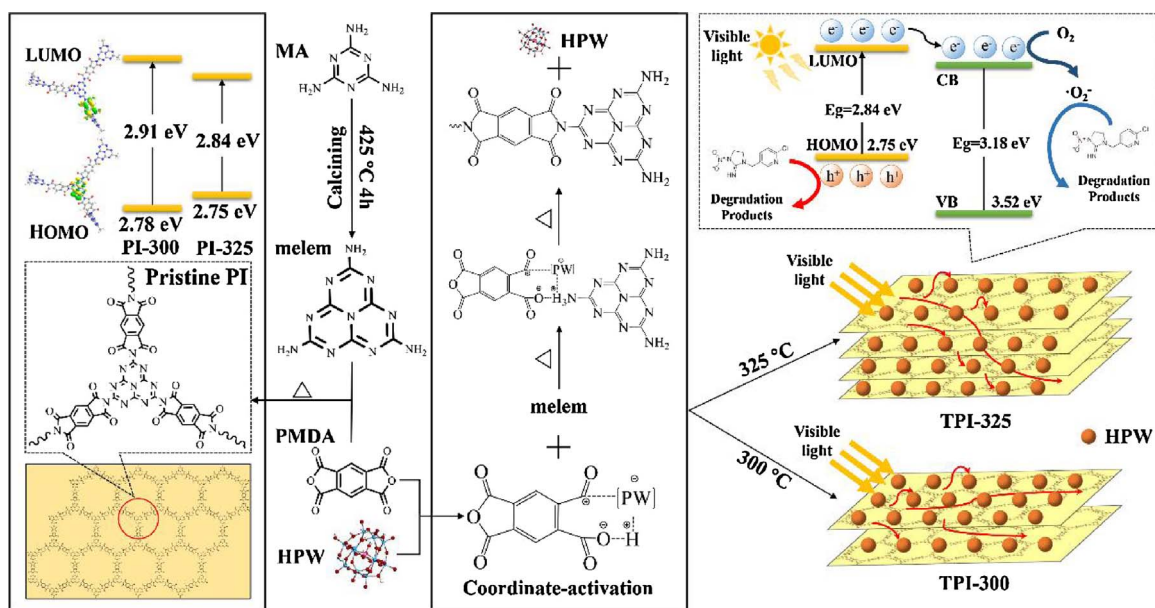
Fig. 3. XPS spectra of (a) survey scan, (b) W4f, (c) N 1s and (d) O 1s spectra of HPW, pristine PI-300, PI-325, 15% TPI-300 and 5% TPI-325.

composites are all higher than that of pristine PI in the dark reaction. In view of the low physical adsorption capacity of the samples, the chemical adsorption between Keggin unit of HPW and imidacloprid molecules may play a role in the photocatalytic reaction [36,37]. In general, the presence of this chemical adsorption will be bound to improve the photocatalytic degradation efficiency of imidacloprid on TPI composites.

3.4. Optical properties of the samples

The optical properties of the samples were investigated by combining UV-vis DRS and PL spectra (Fig. 6). The UV-vis DRS was used to

elucidate the light absorption properties of the samples, and the PL spectra can reflect the separation and transfer efficiency of photo-generated carriers. From Fig. 6(a), all the samples except HPW show excellent visible light absorption ability. The estimated bandgaps of pristine PI-300, PI-325 and HPW are 2.91, 2.84 and 3.18 eV, respectively. For the effect of polymerization temperature, the bandgap of PI-325 with a higher polymerization degree is 0.07 eV narrower than that of PI-300 with a lower polymerization degree because of the more delocalized π electrons along the higher polymerization degree chain, which is consistent with the conclusion in the reference [16]. Besides, the absorption edge of the TPI samples redshift compared with that of corresponding pristine PI, and this redshift mainly come from the



Scheme 1. The fabrication of TPI composites at different polymerization temperature and the photocatalytic mechanism in the TPI composites under visible-light irradiation.

polyimide in the TPI composites for the weak absorption of HPW. This shows that PI should have a higher polymerization degree to lead a narrower bandgap to absorb a wider range of light in the presence of HPW. However, it is noteworthy that the photoabsorption of 5% TPI-325 and 15% TPI-300 is weaker than that of PI-300, especially in the UV region. This may be due to the more multiple reflection and scattering from the PI-300 [49], owing to the differences with the tight block structure of other samples in morphology shown in Fig. 4.

Generally, we all hope to obtain a narrow bandgap photocatalyst for more efficient sunlight utilization, especially visible light. Although the increased polymerization degree can narrow the sample bandgap [16], the photocatalytic activity is affected both by band structure and by the photogenerated carriers separation efficiency of photocatalyst. For this consideration, HPW was introduced as an electron acceptor to promote the separation of photogenerated e^- and h^+ . From Fig. 6(b), for PI-300 and PI-325, the intensity of PI-325 is slight higher than that of PI-300, and a red shift of the PL peak is also occurred. This is because the π -conjugation system extension of PI-325, with a higher polymerization degree, can accelerate the mobility of the charge carriers [22]. By comparing the intensity of pristine PI-325 and 5% TPI-325 composites, the reduced intensity of 5% TPI-325 composites is perfectly presented as expected. This means that the introduction of HPW inhibits the recombination of photogenerated e^- and h^+ for the electron capture capability of Keggin units [36]. As shown in Fig. 3(b), the negative shift of the binding energy of W 4f can confirm this inference. However, for the PL intensity of pristine PI-300 and 15% TPI-300 composites, there is an opposite result compared to the samples prepared at 325 °C. Compared to the intensity of pristine PI-300, the intensity of 15% TPI-300 composites was significantly enhanced after introducing HPW. With the results of FT-IR, XRD, XPS, SEM and TEM, when the polymerization temperature is 300 °C, the samples have relative low polymerization degree and large interlayer spacing, which is not conducive to the transfer of electrons. When HPW as an electronic acceptor and mediator is introduced, HPW will promote the electron transfer, while the relative excess HPW in the laminar layer may also become a new photogenerated e^- and h^+ recombination centers [36]. Accordingly, the enhanced intensity of 15% TPI-300 composites can also be explained reasonably.

3.5. Performance of TPI composites

From Fig. 7(a), the photocatalytic degradation efficiency of imidacloprid is gradually lost in the repetition. From the dark reaction results of each repetition, the adsorption capacity of the photocatalyst to the substrate decrease significantly. However, the HPW content determined by ICP-MS in the photocatalyst after three repetition is 4.20%. Furthermore, from the results of FT-IR and XRD of used photocatalyst, the chemical structure of the used photocatalyst does not change significantly (Fig. 7(b)), except that the crystallinity of the used photocatalyst is slightly reduced (Fig. 7(c)). These results indicate that the loss of photocatalytic activity may be due to the adsorption of excessive imidacloprid and/or intermediates on the photocatalyst rather than the leaching of HPW [36]. Therefore, the used photocatalyst was calcined at 200 °C for 2 h to remove the adsorbed species. It is exciting that the photocatalytic activity of composites is restored obviously. These above results show that TPI composites have excellent recyclability. From Fig. 7(d), compared with commercial P25, the photocatalytic degradation efficiency of 15% TPI-300 and 5% TPI-325 are about 4.58 and 5.13 times of P25. Overall, the TPI composites have a good practical application prospect.

3.6. Possible photocatalytic mechanism

The photocatalytic degradation of organic pollutants on photocatalyst is generally controlled by active species mainly including $\cdot O_2^-$, $\cdot OH$ and h^+ [8]. Herein, the main active species in the involved photocatalytic systems, including the photocatalytic degradation of imidacloprid on TPI composites and corresponding pristine PI, were analyzed by the reactive species trapping experiments and electron spin resonance (ESR) spin-trap technique (Fig. 8).

From Fig. 8(a), the photocatalytic degradation of imidacloprid on PI-300 is obviously suppressed by the addition of 10 mmol Eddate disodium (EDTA-2Na), potassium bromates (KBrO₃) and tertiary butanol (TBA). This indicates that h^+ , $\cdot O_2^-$ and $\cdot OH$ are all the active species in the PI-300 photocatalytic degradation system. After the polymerization temperature is increased and the HPW is introduced, the main active species in the PI-325, 15% TPI-300 and 5% TPI-325 photocatalytic system are all changed to h^+ and $\cdot O_2^-$ with the markedly weakened $\cdot OH$ effects. To further detect reactive oxygen species and determine the photocatalytic mechanism, ESR spin-trap technique

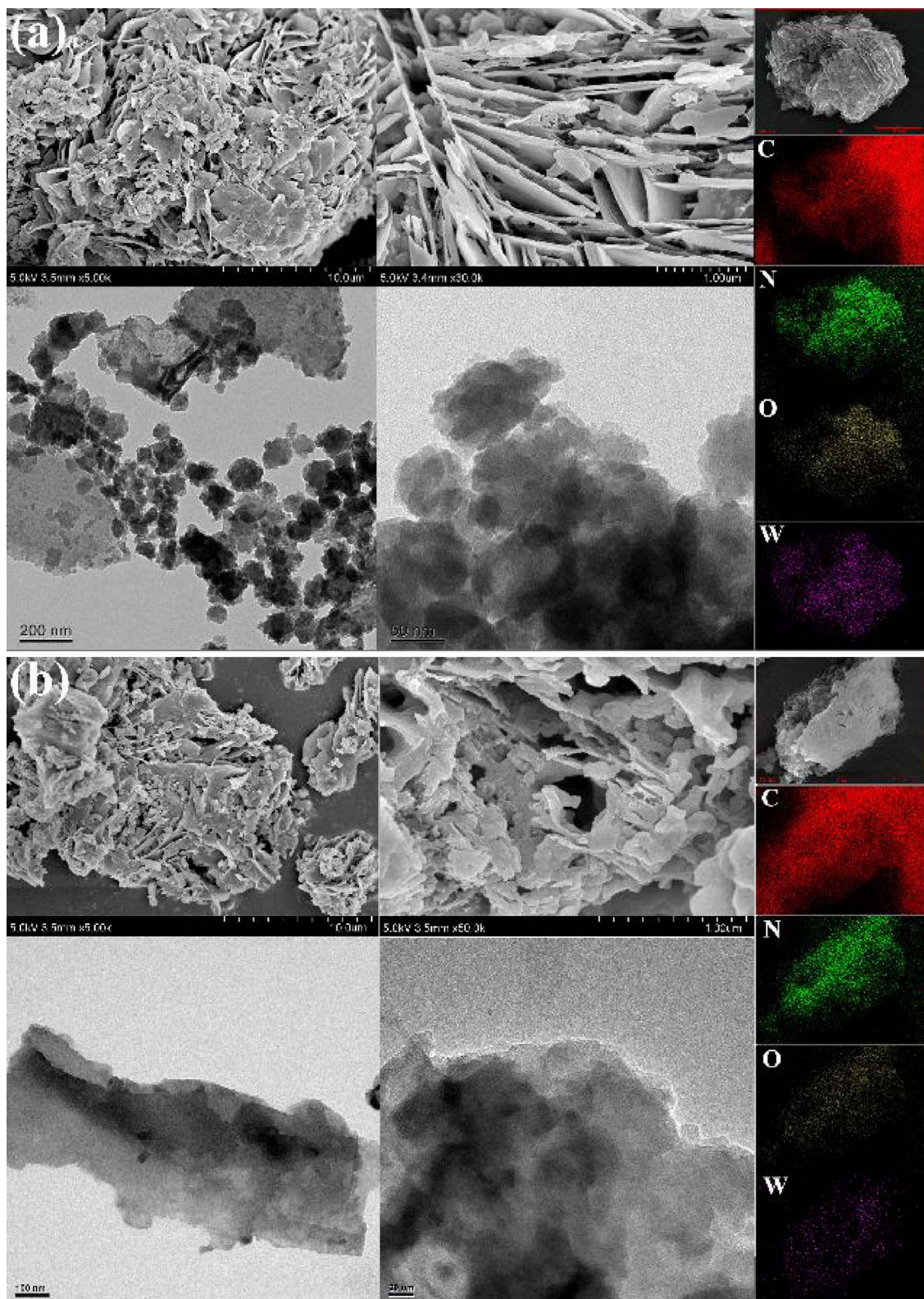


Fig. 4. The images of TEM, SEM and EDX elemental mappings of C, N, O and W for (a) 15%TPI-300 and (b) 5% TPI-325.

was carried out under visible light ($\lambda > 400$ nm) with an irradiation time of 5 min. DMPO (5, 5-dimethyl-1-pyrroline N-oxide) was used to capture the $\cdot\text{O}_2^-$ and $\cdot\text{OH}$ [20]. From Fig. 8(b) and (c), both the four characteristic peaks of DMPO- $\cdot\text{OH}$ and six characteristic peaks of DMPO- $\cdot\text{O}_2^-$ can be clearly determined from the signals of PI-300, PI-325, 15% TPI-300 and 5% TPI-325, respectively. This indicates that the

involved photocatalysts all can originate $\cdot\text{O}_2^-$ and $\cdot\text{OH}$ from the $\text{O}_2/\cdot\text{O}_2^-$ reduction by e^- and $\text{OH}^-/\text{H}_2\text{O}$ oxidation by h^+ , respectively [50]. This capacity is mainly attributed to PI rather than HPW, because HPW cannot be excited by visible light for its wide bandgap ($E_g = 3.18$ eV, as shown in Fig. 6(a)). Moreover, the ability of 5% TPI-325 to generate $\cdot\text{O}_2^-$ and $\cdot\text{OH}$ is strongest, while 15% TPI-300, PI-325 and PI-300

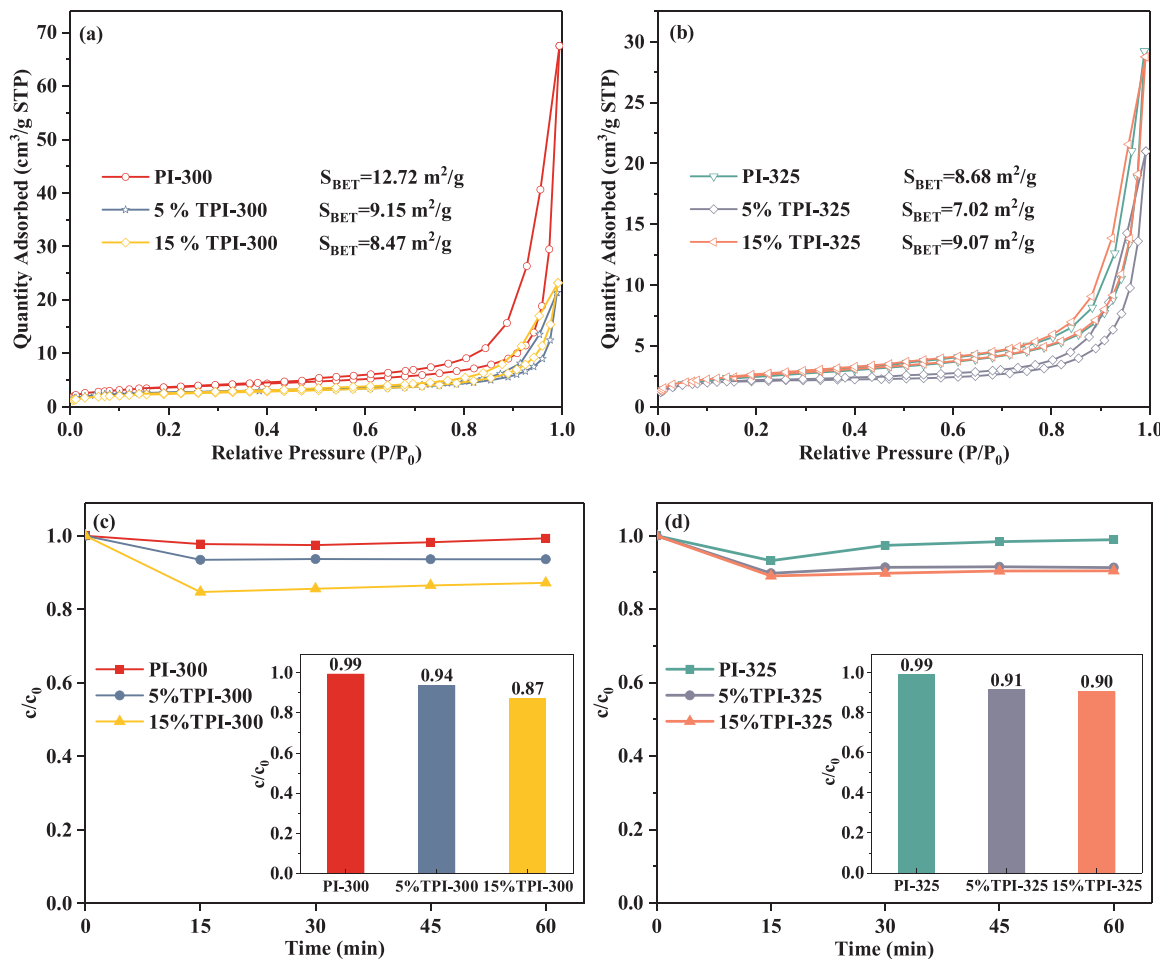


Fig. 5. N_2 adsorption–desorption isotherms and adsorption of imidacloprid on (a, c) PI-300, 5%TPI-300 and 15%TPI-300, and (b, d) PI-325, 5%TPI-325 and 15%TPI-325.

decrease sequentially. This result is positively correlated with the results of photocatalytic degradation of imidacloprid. However, it is not difficult to find that the k is slightly decreased after the addition of TBA (scavenger of $\cdot\text{OH}$) and drastically decreased after the addition of EDTA-2Na (scavenger of h^+). This phenomenon indicates that the h^+ can directly decompose imidacloprid instead of to produce $\cdot\text{OH}$. The enhanced polymerization degree will lead to a negative shift in VB potential [16], and this is confirmed by the VBXPS results shown in Fig. 8(d). Correspondingly, the photocatalytic oxidation capacity of the

h^+ on the VB will be weakened and h^+ may more tend to degrade imidacloprid not to generate $\cdot\text{OH}$. Combined with the photoabsorption and VBXPS results of PI and HPW, the band structures of PI and HPW can be determined as shown in Scheme 1. Thus, the possible photocatalytic mechanism can be proposed.

Typically, the mechanism of photocatalytic degradation of organic pollutants on photocatalyst can be divided into the following steps, including the photoexcitation of photocatalyst, photogenerated carrier transfer and reaction of active species. From the results of UV–vis DRS

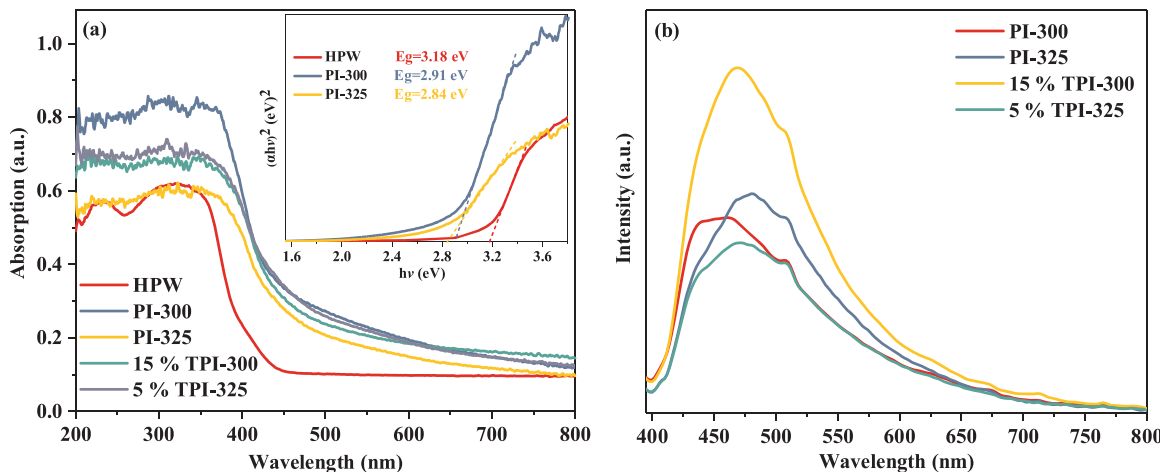


Fig. 6. UV-vis diffuse reflectance spectra (a) of the samples, and PL spectra (b) of pristine PI-300, PI-325, 15% TPI-300 and 5% TPI-325 composites. The inset in (a) is the plots of $(\alpha h\nu)^2$ vs photon energy (hv) for the band gap energies of the samples.

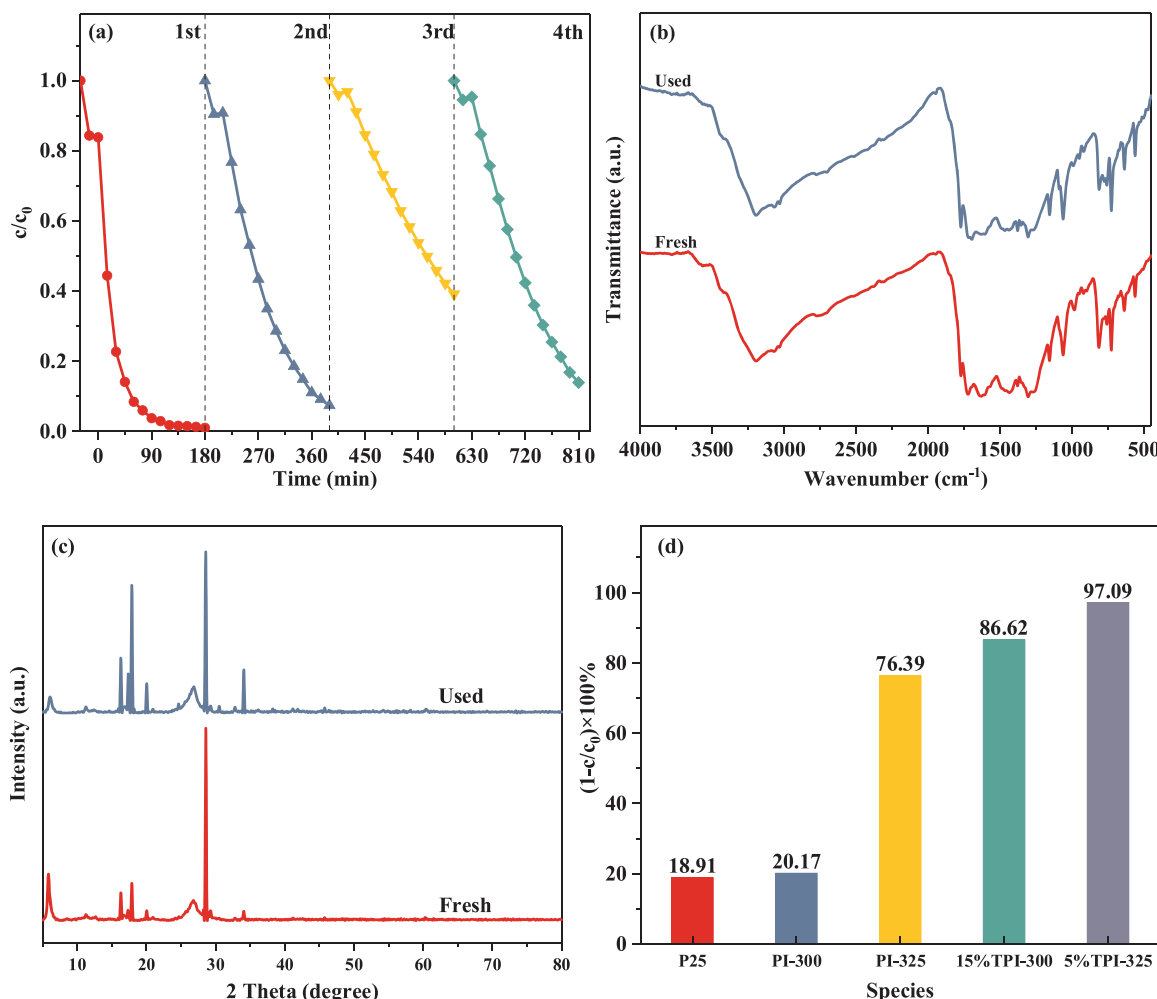
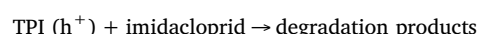
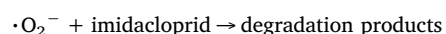
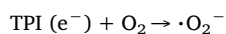
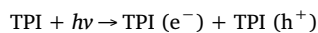


Fig. 7. The recyclability test (a) for 5% TPI-325 (the photocatalyst concentration 2.5 g L^{-1} , imidacloprid concentration 20 mg L^{-1}), FT-IR spectra (b) and XRD patterns (c) of fresh and used 5% TPI-325. (d) The photocatalytic efficiency of commercial P25, pristine PI-300 and PI-325, 15% TPI-300 and 5% TPI-325 in 3 h.

(Fig. 6(a)), both pristine PI and TPI composites have visible light absorption, while HPW has only UV light absorption. Therefore, the e^- - h^+ pairs are only generated on the PI under visible light irradiation for the wide bandgap of HPW. As shown in Scheme 1, because of the introduction of HPW into TPI composites, HPW will serve as an electron acceptor and mediator to promote the separation of e^- and h^+ and the electron transfer in the photocatalytic system [36,48]. As the electron mediator, HPW will promote the surface and interlayer electron transfer of PI. As the electron acceptor, the photogenerated e^- will be instantly transferred into unoccupied W5d orbits of the Keggin unit by HPW, and HPW will be reduced to form the heteropoly blue (HPB) [51,52]. HPB can be easily reoxidized back to its oxidation state by dioxygen with the generation of $\cdot\text{O}_2^-$ [51,52]. Overall, the results of the reactive species trapping experiments, photocatalytic tests and characterization show: (i) the introduction of HPW will promote the polymerization between amine and anhydride precursors during the in-situ polymerization process of TPI composites. (ii) the increased photocatalytic efficiency of TPI composites may be due to the common effects of increased photo-generated e^- and h^+ separation efficiency, the high visible light utilization efficiency and chemical adsorption capacity. Based on the above analysis, the proposed photocatalytic degradation process of imidacloprid on TPI composites is as follows.



4. Conclusions

A series of TPI composites are successfully synthesized using in-situ solid-state polymerization strategy. The introduction of HPW has significantly promoted the polymerization between amine and anhydride precursors. The TPI composites with suitable HPW content exhibit desired enhanced photocatalytic degradation efficiency of imidacloprid under visible light irradiation. The enhanced photocatalytic activity is attributed to the enhancement of the polymerization reaction, the photogenerated e^- - h^+ separation efficiency and visible-light utilization efficiency after the introduction of HPW. The k of 15% TPI-300 and 5% TPI-325 are about 10.33 and 2.42 times of the corresponding pristine PI, respectively. The chemical adsorption between Keggin unit of HPW and imidacloprid molecules may play a more positive role in the photocatalytic reaction. Compared with commercial P25, the photocatalytic degradation efficiency of 15% TPI-300 and 5% TPI-325 are about 4.58 and 5.13 times of P25 under visible light irradiation, respectively. The TPI composites have a good practical application prospect. In summary, this investigation about the effect of HPW introduction on the in-situ solid-state condensation and photocatalytic activity of TPI composites may be broadly used in the synthesis of the conjugated polymer-based photocatalyst for the abundant resources of amine and anhydride monomers, also in other photocatalytic

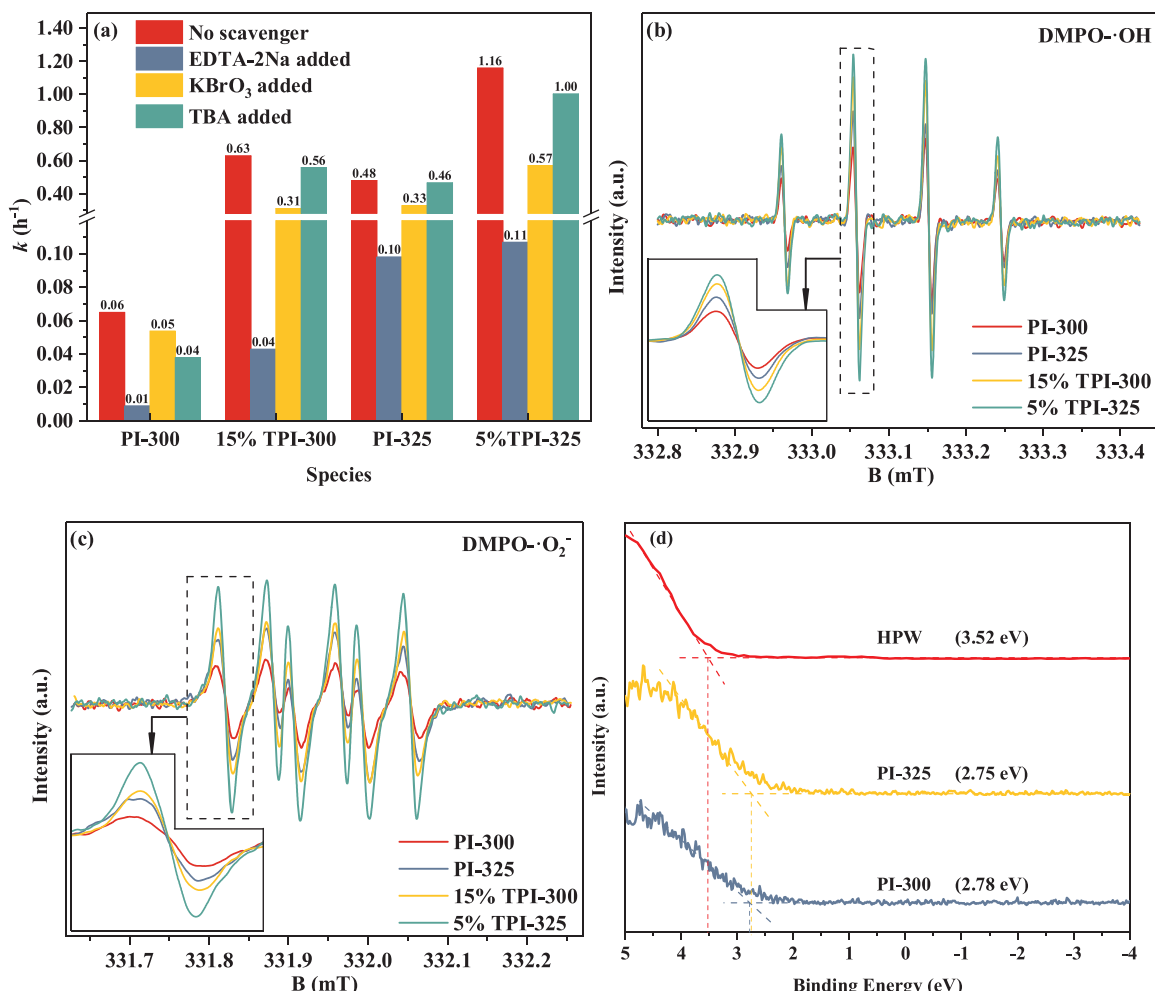


Fig. 8. Effects of (a) different scavengers to photocatalytic degradation of imidacloprid and ESR signals of the (b) DMPO-·OH and (c) DMPO-·O₂⁻ for 15% TPI-300, 5% TPI-325 and corresponding pristine PI under visible light irradiation, and (d) VBXPS spectra of HPW and pristine PI.

application areas.

Acknowledgements

All authors acknowledge Prof. Changgen Feng and Dr. Qiang Gan from Beijing Institute of Technology for their help on the characterization of photocatalysts.

Appendix A. Supplementary data

Supplementary data associated with this article can be found, in the online version, at <https://doi.org/10.1016/j.apcatb.2018.01.004>.

References

- [1] J. Xiao, Y. Xie, H. Cao, *Chemosphere* 121 (2014) 1–17.
- [2] C.A. Morrissey, P. Mineau, J.H. Devries, F. Sanchez-Bayo, M. Liess, M.C. Cavallaro, K. Liber, *Environ. Int.* 74 (2015) 291–303.
- [3] K. Jardak, P. Drogui, R. Daghbir, *Environ. Sci. Pollut. Res.* 23 (2016) 3195–3216.
- [4] S.H.S. Chan, T. Yeong Wu, J.C. Juan, C.Y. Teh, *J. Chem. Technol. Biotechnol.* 86 (2011) 1130–1158.
- [5] H. Sun, S. Liu, S. Liu, S. Wang, *Appl. Catal. B Environ.* 146 (2014) 162–168.
- [6] J. Zhang, S. Wageh, A. Al-Ghamdi, J. Yu, *Appl. Catal. B Environ.* 192 (2016) 101–107.
- [7] C. Li, Y. Xu, W. Tu, G. Chen, R. Xu, *Green Chem.* 19 (2017) 882–899.
- [8] W. Ong, L. Tan, Y.H. Ng, S. Yong, S. Chai, *Chem. Rev.* 116 (2016) 7159–7329.
- [9] D. Masih, Y. Ma, S. Rohani, *Appl. Catal. B Environ.* 206 (2017) 556–588.
- [10] X. Wang, S. Blechert, M. Antonietti, *ACS Catal.* 2 (2012) 1596–1606.
- [11] Y. Xiao, B.T. Low, S.S. Hosseini, T.S. Chung, D.R. Paul, *Prog. Polym. Sci.* 34 (2009) 561–580.
- [12] D. Liaw, K. Wang, Y. Huang, K. Lee, J. Lai, C. Ha, *Prog. Polym. Sci.* 37 (2012) 907–974.
- [13] S. Chu, Y. Wang, Y. Guo, P. Zhou, H. Yu, L. Luo, F. Kong, Z. Zou, *J. Mater. Chem.* 22 (2012) 15519–15521.
- [14] S. Chu, Y. Wang, Y. Guo, J. Feng, C. Wang, W. Luo, X. Fan, Z. Zou, *ACS Catal.* 3 (2013) 912–919.
- [15] L. Lin, P. Ye, C. Cao, Q. Jin, G. Xu, Y. Shen, Y. Yuan, *J. Mater. Chem. A* 3 (2015) 10205–10208.
- [16] S. Chu, Y. Wang, C. Wang, J. Yang, Z. Zou, *Int. J. Hydrog. Energy* 38 (2013) 10768–10772.
- [17] C. Ma, H. Zhu, J. Zhou, Z. Cui, T. Liu, Y. Wang, Y. Wang, Z. Zou, *Dalton Trans.* 46 (2017) 3877–3886.
- [18] C. Wang, Y. Guo, Y. Yang, S. Chu, C. Zhou, Y. Wang, Z. Zou, *ACS Appl. Mater. Interfaces* 6 (2014) 4321–4328.
- [19] J. Dasgupta, J. Sikder, S. Chakraborty, U. Adhikari, V.P. Reddy, B.A. Mondal, S. Curcio, *ACS Sustain. Chem. Eng.* 5 (2017) 6817–6826.
- [20] P. Meng, H. Heng, Y. Sun, X. Liu, *Appl. Surf. Sci.* 428 (2018) 1130–1140.
- [21] T. Yan, M. Li, X. Wang, M. Sun, H. Liu, Q. Wei, W. Xu, B. Du, *Appl. Surf. Sci.* 340 (2015) 102–112.
- [22] C. Ma, J. Zhou, Z. Cui, Y. Wang, Z. Zou, *Sol. Energy Mater. Sol. Cells* 150 (2016) 102–111.
- [23] C. Ma, J. Zhou, H. Zhu, W. Yang, J. Liu, Y. Wang, Z. Zou, *ACS Appl. Mater. Interface* 7 (2015) 14628–14637.
- [24] J. Li, X. Jiang, L. Lin, J. Zhou, G. Xu, Y. Yuan, *J. Mol. Catal. A Chem.* 406 (2015) 46–50.
- [25] Y. Gong, H. Yu, S. Chen, X. Quan, *RSC Adv.* 5 (2015) 83225–83231.
- [26] J. Yang, D. Wang, H. Han, C. Li, *Acc. Chem. Res.* 46 (2013) 1900–1909.
- [27] R. Marschall, *Adv. Funct. Mater.* 24 (2014) 2421–2440.
- [28] H. Heng, Q. Gan, P. Meng, X. Liu, *RSC Adv.* 6 (2016) 73301–73307.
- [29] A. Hiskia, M. Ecke, A. Troupis, A. Kokorakis, H. Hennig, E. Papaconstantinou, *Environ. Sci. Technol.* 35 (2001) 2358–2364.
- [30] G.W. Wang, Y.B. Shen, X.L. Wu, *Eur. J. Org. Chem.* 2008 (2010) 4367–4371.
- [31] A. Jha, A.C. Garade, S.P. Mirajkar, C.V. Rode, *Ind. Eng. Chem. Res.* 51 (2012) 3916–3922.
- [32] S. Wang, G. Yang, *Chem. Rev.* 115 (2015) 4893–4962.

[33] Y. Zhu, M. Zhu, L. Kang, F. Yu, B. Dai, *Ind. Eng. Chem. Res.* 54 (2015) 2040–2047.

[34] H. Heng, Q. Gan, P. Meng, X. Liu, *J. Alloy Compd.* 696 (2017) 51–59.

[35] D. Fei, P. Wei, *J. Photochem. Photobiol. B* 147 (2015) 24–36.

[36] K. Li, L. Yan, Z. Zeng, S. Luo, X. Luo, X. Liu, H. Guo, Y. Guo, *Appl. Catal. B Environ.* 156–157 (2014) 141–152.

[37] J. He, H. Sun, S. Indrawirawan, X. Duan, M.O. Tade, S. Wang, *J. Colloid Interface Sci.* 456 (2015) 15–21.

[38] C.L. Marchena, R.A. Frenzel, S. Gomez, L.B. Pierella, L.R. Pizzio, *Appl. Catal. B Environ.* 130–131 (2013) 187–196.

[39] G. Marci, E.I. García-López, F.R. Pomilla, L.F. Liotta, L. Palmisano, *Appl. Catal. A* Gen. 528 (2016) 113–122.

[40] Z. Lan, G. Zhang, X. Wang, *Appl. Catal. B Environ.* 192 (2016) 116–125.

[41] L. Huang, H. Xu, Y. Li, H. Li, X. Cheng, J. Xia, Y. Xu, G. Cai, *Dalton Trans.* 42 (2013) 8606–8616.

[42] Y. Liao, J. Weber, C.F.J. Faul, *Macromolecules* 48 (2015) 2064–2073.

[43] U.B. Nasini, V.G. Bairi, S.K. Ramasahayam, S.E. Bourdo, T. Viswanathan, A.U. Shaikh, *J. Power Sources* 250 (2014) 257–265.

[44] J. Liu, S. Xie, Z. Geng, K. Huang, L. Fan, W. Zhou, L. Qiu, D. Gao, L. Ji, L. Duan, L. Lu, W. Li, S. Bai, Z. Liu, W. Chen, S. Feng, Y. Zhang, *Nano Lett.* 16 (2016) 6568–6575.

[45] Y. Yu, X. Zhong, H. Su, A. Serra, *Polymer* 51 (2010) 1563–1571.

[46] H. Li, W. Tu, Y. Zhou, Z. Zou, *Adv. Sci.* 3 (2016) 1500389.

[47] Z. Peng, Y. Jiaguo, M. Jaroniec, *Adv. Mater.* 26 (2014) 4920–4935.

[48] X. Yang, F. Qian, Y. Wang, M. Li, J. Lu, Y. Li, M. Bao, *Appl. Catal. B Environ.* 200 (2017) 283–296.

[49] S. Tu, H. Huang, T. Zhang, Y. Zhang, *Appl. Catal. B Environ.* 219 (2017) 550–562.

[50] H. Huang, S. Tu, C. Zeng, T. Zhang, A.H. Reshak, Y. Zhang, *Angew. Chem. Int. Ed.* 56 (2017) 11860–11864.

[51] F. Ma, T. Shi, J. Gao, L. Chen, W. Guo, Y. Guo, S. Wang, *Colloid Surf. A* 401 (2012) 116–125.

[52] J. Li, W. Kang, X. Yang, X. Yu, L. Xu, Y. Guo, H. Fang, S. Zhang, *Desalination* 255 (2010) 107–116.